Design and Chatter Prediction Analysis of a Duplex Face Turning Machine for Manufacturing Disk-like Workpieces

Article *in* International Journal of Machine Tools and Manufacture · January 2019

DOI: 10.1016/j.ijmachtools.2019.01.006

CITATIONS
0

READS
29

4 authors, including:

Kun Bai
Huazhong University of Science and Technology
40 PUBLICATIONS 215 CITATIONS

SEE PROFILE

Kok-Meng Lee
Georgia Institute of Technology
134 PUBLICATIONS 794 CITATIONS

SEE PROFILE

International Journal of Machine Tools and Manufacture 140 (2019) 12–19

Contents lists available at ScienceDirect

International Journal of Machine Tools and Manufacture

journal homepage: www.elsevier.com/locate/ijmactool

Design and chatter prediction analysis of a duplex face turning machine for manufacturing disk-like workpieces

Kun Bai[a,*], Jialin Qin[a], Kok-Meng Lee[a,b,**], Bingjie Hao[a]

[a] State Key Lab of Digi. Manuf. Equip. and Tech., Huazhong Univ. of Sci. and Tech., Wuhan 430074, China
[b] Woodruff Sch. of Mech. Eng., Georgia Inst. of Tech., Atlanta, GA 30332, USA

ABSTRACT

Simultaneous, parallel or double-sided machining can increase the metal-removal-rate (MRR) of hard-to-cut materials. This paper presents a direct-drive duplex-face-turning (DFT) machine for manufacturing thin-walled disk-like components characterized by a very large diameter-to-thick ratio, which allows simultaneous cutting of opposite sides to improve productivity and mitigate workpiece deformations/vibrations during machining. The unique dynamic characteristics on the cutting interface between the thin-walled disk and the two cutters, however, present some challenges in chatter prediction and process parameter optimization. To address these challenges, a multi-dimensional chatter stability analysis method based on a conceptually straightforward modeling approach in terms of the major oblique cutting parameters is presented, where the dynamic effects of both the workpiece and two cutters in addition to the insert geometries are taken into considerations in the formulation of the DFT process. The proposed chatter stability analysis is numerically illustrated and experimentally validated. The relative merit of the direct-drive DFT process has been experimentally evaluated for machining thin-walled hard-to-machine compressor disks by comparing symmetric and non-symmetric DFT operations with single-sided face-turning, along with an example that illustrates a quick guide for nonsymmetrical DFT in the specified speed range.

1. Introduction

Machining of thin-walled aero-engine components with excellent quality and superior service performance are challenging tasks. The continued interests to push forward machining accuracy and productivity have motivated the advanced manufacturing industry to explore new methods and develop new machining equipments. One of the typical hard-to-machine components in aero-engines are the compressor disks featured with large diameter (up to 1 m) and small thickness (less than 1 mm). Manufacturing of such disk-like workpieces (WPs) on a conventional turning machine is challenging. Complex fixtures are required and the cutter normal force (usually applied on one side of the WPs) can cause deformations and vibrations rendering poor precision and quality in final products [1]. These challenges call for the development of new duplex face turning (DFT) machines capable of machining both sides of thin-walled disk-like WPs, which can not only increase the metal removal-rate (MRR) but also mitigate deformations and vibrations due to unbalanced cutting conditions. Because of the complex DFT tool-WP dynamics and chatter characteristics, the attractive advantages of the DFT process are underexploited. For the above reasons, this paper analyzes the DFT dynamic cutting process, and offers a chatter stability analysis method for finding optimal machining parameters.

Chatter vibrations caused by instability in the cutting processes have been extensively studied for different metal cutting processes [2~6]. As one of the commonly used metal removal process for a variety of products, the chatter stability of the turning process has also been widely investigated. Rao and Shin [7] proposed a comprehensive model of three-dimensional dynamic cutting force system for chatter prediction in turning. Budak and Ozlu [8] also presented an analytical multi-dimensional model to predict the stability limits in turning and boring processes, where major parameters of the process geometry such as oblique angle, approach angle and nose radius were considered. While most studies on turning mainly focused on circumferential surface machining (cutter fed along axial direction), Clancy and Shin [9] formulated the dynamic cutting model for face-turning process (cutter fed along radial direction), which presented a different formation of chip load; and a chatter prediction model was then developed and verified experimentally. Recently, simultaneous/parallel machining with extra cutters to increase the MRR have been investigated for lathe turning [10~11] and double-sided milling [12~13]. Budak [14] developed frequency and time domain models for the stability analysis of an orthogonal parallel turning operation; and the results show the stability could be increased due to dynamic interaction between the tools creating an absorber effect on each other. Azvar and Budak [15] then developed a general multidimensional stability model for different parallel turning strategies where tools can cut a shared surface or different surfaces of a WP; and the main parameters of process geometry such as side edge, cutting angle and nose radii of the tools were

* Corresponding author. State Key Lab of Digi. Manuf. Equip. and Tech., Huazhong Univ. of Sci. and Tech., Wuhan, 430074, China
** Corresponding author. Georgia Inst. of Tech., Atlanta, GA 30332, USA.
E-mail addresses: kbai@hust.edu.cn (K. Bai), kokmeng.lee@me.gatech.edu (K.-M. Lee).

https://doi.org/10.1016/j.ijmachtools.2019.01.006
Received 22 October 2018; Received in revised form 24 January 2019; Accepted 28 January 2019
Available online 30 January 2019
0890-6955/

included in the analysis. Ozturk et al. [16] analyzed the effect of natural frequency of the tools in chatter stability of parallel turning operations and proposed methods for improving the system stability by changing the system configurations.

While existing studies on simultaneous/parallel turnings mainly focusing on circumferential surface machining of rod-type WPs, the dynamic analysis and the chatter prediction of the DFT machining of disk-like WPs with unique tool-WP interface (mirror-imaged face turning) and dynamic interactions between opposite cutters and the disk-like WP (featured with totally different dynamic stiffnesses in axial and radial directions) are still underexploited. Based on a recently developed DFT machine and the cutting force model previously developed for single-sided face turning [9], a chatter stability analysis method for DFT is developed in this paper. The remainder of this paper offers the following:

- The design configuration of a lathe machine for DFT of thin-walled disk-like WPs is discussed. As will be shown, the proposed DFT machine is capable of eliminating the deformations of the thin-walled disks during the machining process without the needs of complex clamping fixtures to accommodate WP geometry.
- A three-dimensional model characterizing the cutting forces between a disk-like WP and two cutters in DFT operation is formulated, where the geometric parameters of the oblique cutting process are taken into account. A frequency domain method for analyzing the chatter stability of the DFT process is proposed. Specifically, the dynamics of both the tools and the thin-walled WP are included in the analysis.
- Built upon the DFT cutting force and chatter prediction models, stability lobe diagrams representing the critical machining parameters of the DFT (spindle speed and two depth-of-cuts, DOCs) are computed, which are experimentally validated with cutting tests conducted on a DFT machine. Results of numerical and experimental investigations based on the machining of titanium-alloy compressor disks are discussed.

2. DFT machine design and chatter prediction

Fig. 1 shows two different lathe design configurations for face-turning process of a disk-like WP; conventional single-sided (Fig. 1a) and traditional belt-driven duplex (Fig. 1b) face-turning. Vibrations caused by unbalanced spindle loads and low productivity due to the needs to reconfigure the fixtures for supporting the opposite side are well-known problems associated with conventional single-side facing-turning (SSFT). Unlike the SSFT that requires complicated fixtures for accommodating the WP geometry in order to mitigate the deformations due to the unbalanced cutter normal forces, the duplex face turning (DFT) with two cutters (CTs) applied on both sides of the WP take advantages of the mirror-imaged cutting to reduce potential deformations and improve MRR. However, traditional belt-driven DFT machines rely on gear-reducers and timing-belts to transmit torques from high-speed electric motors, where the long transmission chain introduces unavoidable mechanical wears/tears resulting in significant disturbances and vibrations during cutting.

Fig. 1(c) illustrates a direct-drive DFT (DD-DFT) machine composed of a DD spindle motor [1718] and two CTs (on opposite sides of the WP). As shown in Fig. 1(c), the spindle motor has a hollow rotor which allows the WP to be clamped at its outer perimeter, which eliminates the need of complex fixtures and permits relative large room in the vicinity of cutting area for installation of sensors for online monitoring of the machining process. Each CT is mounted on a two-DOF translation stage moving along the X (feed) and the Z (depth-of-cut) directions of the WP. The pair of CTs is simultaneously controlled in the feed direction to align the cutting points on both sides of the WP during the machining process; and the CT structures are symmetric with similar stiffness to assure the static normal forces applied on the WP are cancelled out during the machining process to eliminate deformations. In order to exploit the characteristics of the DFT process and determine the optimal machining parameters for the DFT machine, analytical models characterizing the interactions between the disk-like WP and the cutters on opposite sides are formulated and chatter stability analysis method is proposed for DFT process in the following subsections.

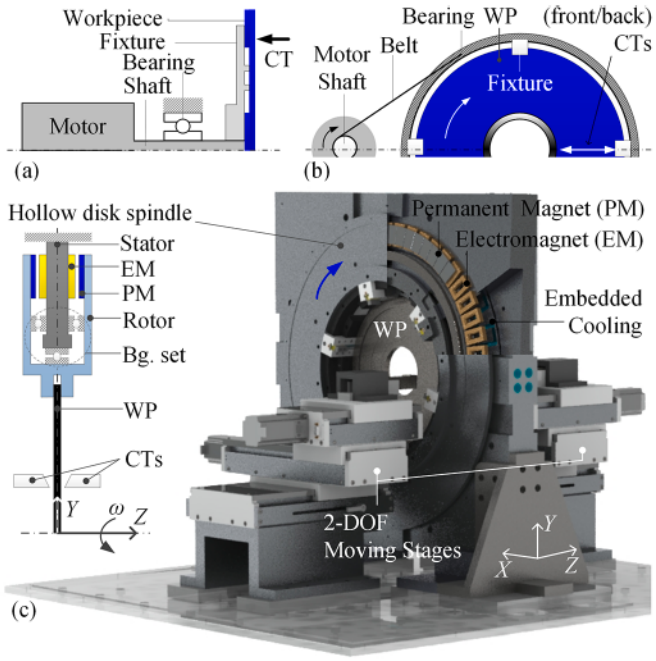

Fig. 1. Lathe machines for manufacturing disc-like WP. (a) Conventional single-sided face-turning (SSFT). (b) Traditional belt-driven duplex face-turning. (c) Direct-drive DFT machine.

2.1. Formulation of DFT dynamic force model

Fig. 2 schematically illustrates the parameters and variables at the cutting interfaces of a typical DFT where the WP interacts with two CTs. As in Fig. 1(c), the global XYZ reference coordinates is defined at the center of the motor. The WP is rotated at speed n (rpm) in Fig. 2(a) where (f_X, f_Y, f_Z) are the force components; and v is the common feedrate of both CTs with DOCs $b_{\pm}$ (where "+" and "–" indicate the left and right sides when viewing in the $+X$ direction). With the free-body diagrams in Fig. 2(c), the cutting system dynamics is modeled using a lumped-parameter (mass-spring-damper) approach, where $\mathbf{r}$ and $\mathbf{f}$ are

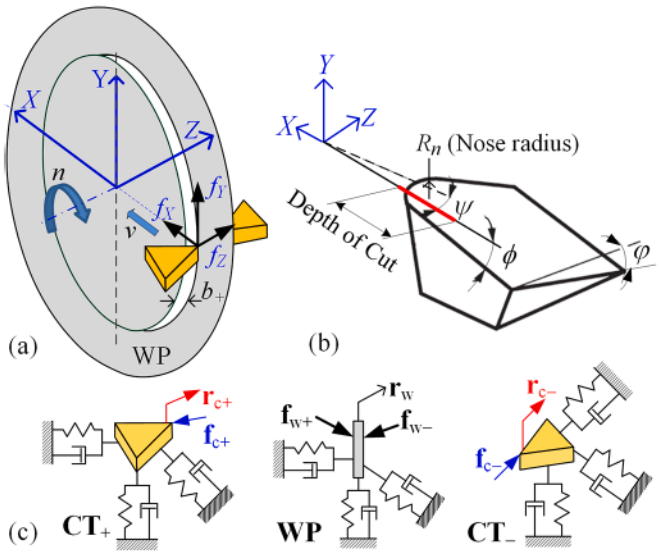

Fig. 2. Schematics illustrating DFT (a) Reference coordinates. (b) Geometric parameters. (c) Free-body diagram, "+" and "–" indicate the left and right sides.

the vibratory displacement and applied/reaction-force vectors respectively; and the subscripts "c ± and w ± " denote the "CT ± and WP". As illustrated in Fig. 2(a), the motion/cutting-force directions of the right-CT can be treated as a mirror image of the left-CT on the *XY*-plane. In other words, their motions relative to the WP have the same signs in their respective *X* and *Y* directions but opposite in the *Z* direction. For clarity in the following discussions, the cutting forces acting on the WP will be derived for the left-CT with its local coordinate axes parallel to *XYZ* (and thus to that of the WP). The dynamics of the right-CT can then be deduced from the mirror image that can be characterized by the transformation matrix [S]:

$$[\mathbf{S}] = [\mathbf{S}]^{-1} = \begin{bmatrix} [\mathbf{I}]_{2\times 2} & \mathbf{0}_{2\times 1} \\ \mathbf{0}_{1\times 2} & -1 \end{bmatrix} \tag{1}$$

Neglecting the tool wear and process damping, the cutting force components on the CT rake-face are proportional to the (normal, frictional) pressure coefficients (K_f, K_n) and the chip cross-sectional area (bh where h is the chip load). Using the geometrical parameters [7,9] defined in Fig. 2(b) where (ϕ,ψ,φ) are the (cutting edge, inclination, normal rake) angles of CT, the force f acting on the WP by a CT during face-turning can be written as

$$\frac{\mathbf{f}}{bh} = \mathbf{k} = \begin{bmatrix} K_X \\ K_Y \\ K_Z \end{bmatrix} = [\mathbf{\Gamma}(\phi, \psi, \varphi)] \begin{bmatrix} K_f C_\eta \\ K_n \\ K_f S_\eta \end{bmatrix} \tag{2}$$

In (2), the 3 × 3 matrix $[\mathbf{\Gamma}(\phi, \psi, \varphi)] = [\mathbf{\Gamma}_Y(\psi)][\mathbf{\Gamma}_X(\phi)][\mathbf{\Gamma}_Z(\varphi)]$ transforms the tool forces to the XYZ reference frame; and C_η and S_η are the trigonometric cosine and sine functions of the chip flow angle η.

In turning, regenerative chatter occurs when cutting a surface modulated from its previous cut, the dynamic effects of which can be accounted for by including the appropriate terms in the instantaneous chip load h in (3) where h_0 is the static chip load and the cross-coupling factor σ represents a change in chip load due to the vibration in the axial direction [9]:

$$\Delta h = h - h_0 = [1 \quad 0 \quad \sigma]\Delta\mathbf{r} \tag{3}$$

where $\Delta\mathbf{r} = [\Delta x, \ \Delta y, \ \Delta z]^T = \Delta\mathbf{r}_c - \Delta\mathbf{r}_w$

and $\Delta\mathbf{r}_c = \mathbf{r}_c(t) - \mathbf{r}_c(t-T); \Delta\mathbf{r}_w = \mathbf{r}_w(t) - \mathbf{r}_w(t-T)$

As shown in Fig. 3, $\mathbf{r}(t-T)$ and $\mathbf{r}(t)$ in (3) are the vibratory displacement vectors for the previous and current revolutions (with period $T = 60/n$) respectively. For a square or diamond-shaped insert machining above the nose radius R_n,

$$\sigma b = R_n(1 - \sin\psi) + (b - R_n)\tan\psi \tag{4}$$

Substituting (3) into (2), yields

$$\mathbf{f} - \mathbf{f}_0 = \mathbf{kb}\Delta\mathbf{r} \tag{5}$$

where $\mathbf{f}_0 = bh_0\mathbf{k}$ and $\mathbf{b} = [b \quad 0 \quad \sigma b]$

Equations (4) and (5) suggest that $\mathbf{b}$ depends on $b_\pm$ and $\sigma_\pm$. For DFT, the cutting forces applied from both sides can be expressed as

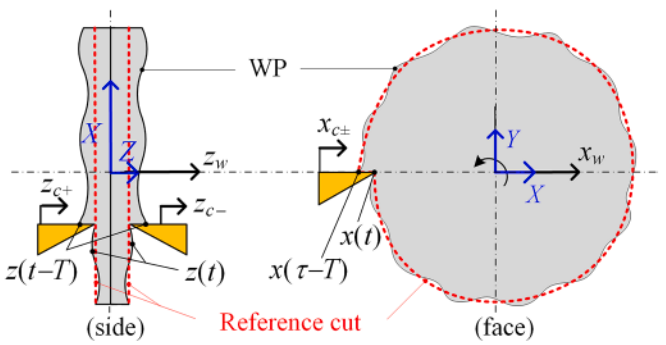

Fig. 3. Schematics illustrating cutting dynamics.

$$\mathbf{f}_{w+} = \mathbf{f}_+ - \mathbf{f}_{0+} = \mathbf{kb}_+\Delta\mathbf{r}_+ \tag{6}$$

$$[\mathbf{S}]\mathbf{f}_{w-} = [\mathbf{S}](\mathbf{f}_- - \mathbf{f}_{0-}) = \mathbf{kb}_-([\mathbf{S}]\Delta\mathbf{r}_-)$$

The above pair of equations can be rewritten as

$$\mathbf{f}_{w\pm} = [\mathbf{A}_\pm]\Delta\mathbf{r}_\pm \tag{7}$$

where $[\mathbf{A}_+] = \mathbf{kb}_+$ and $[\mathbf{A}_-] = [\mathbf{S}]^{-1}\mathbf{kb}_-[\mathbf{S}]$.

The significance of the DFT on the WP motion $\Delta\mathbf{r}_w = [\Delta x_w \ \Delta y_w \ \Delta z_w]^T$ is best illustrated by considering an ideal symmetric cutting ($b_\pm = b$, $\sigma_\pm = \sigma$, $\Delta\mathbf{r}_c = [\Delta x_c \ \Delta y_c \ \Delta z_c]^T$) using (7):

$$\begin{aligned}\mathbf{f}_{w+} + \mathbf{f}_{w-} &= \mathbf{kb}\Delta\mathbf{r}_+ - ([\mathbf{S}]^{-1}\mathbf{kb})([\mathbf{S}]\Delta\mathbf{r}_-) \\ &= 2\begin{bmatrix} bK_X\Delta x_c + \sigma bK_X\Delta z_c \\ bK_Y\Delta x_c + \sigma bK_Y\Delta z_c \\ 0 \end{bmatrix} - 2\begin{bmatrix} bK_X\Delta x_w \\ bK_Y\Delta x_w \\ \sigma bK_Z\Delta z_w \end{bmatrix}\end{aligned}$$

As shown above, the forces generated by the symmetrical CT motions (including static displacement and vibratory displacement) are cancelled out along the Z (out-of-plane) direction but doubled along the *X* (feed) and the *Y* (cutting) directions. The net force along the *Z* direction is due to the vibratory motion of the WP about its steady-state displacement.

2.2. Chatter prediction for DFT

For chatter prediction of the DFT, the dynamic forces relative to the static equilibrium are derived in frequency domain. From the Newton's 3rd law of motion, the dynamic forces acting on both sides of the DFT in Laplace domain can be obtained as (8) based on (7) and (3):

$$\mathbf{F}_{w\pm}(s) = -\mathbf{F}_{c\pm}(s) = (1 - e^{-sT})[\mathbf{A}_\pm](\mathbf{R}_{c\pm}(s) - \mathbf{R}_w(s)) \tag{8}$$

In (8) and subsequent derivations, the capitalized vector **F** represents the Laplace transform of the force vector **f** with components in Fig. 2(c); and **R** represents the displacement vector **r** defined in (3). Equation (7) provide a general form for formulating the dynamic relationship between the cutting forces and vibratory displacements of the CT ± and WP systems, which can be characterized respectively by the transfer functions $\mathbf{G}_\pm$ and **H**:

$$\mathbf{R}_{c\pm} = [\mathbf{G}_\pm]\mathbf{F}_{c\pm} \text{ and } \mathbf{R}_w = [\mathbf{H}](\mathbf{F}_{w+} + \mathbf{F}_{w-}) \tag{9}$$

In (9), $\mathbf{G}_- = [\mathbf{S}]^{-1}\mathbf{G}_+[\mathbf{S}]$because of the mirror-imaged CTs. The CT ± / WP dynamic relationship is graphically illustrated by the block diagram shown in Fig. 4 where $\hat{\mathbf{F}}_\pm$represents un-modeled force disturbance. For a DFT system where the three orthogonal axes are dynamically independent of each other,

$$[\mathbf{G}_+] = [\mathbf{G}_-] = diag(G_X, G_Y, G_Z) \tag{10}$$

$$[\mathbf{H}] = diag(H_X, H_Y, H_Z)$$

From equations (8)–(10), we have

$$\begin{bmatrix} \mathbf{F}_{w+} \\ \mathbf{F}_{w-} \end{bmatrix} = -(1 - e^{-sT})\begin{bmatrix} [\mathbf{A}_+][\mathbf{H} + \mathbf{G}_+] & [\mathbf{A}_+][\mathbf{H}] \\ [\mathbf{A}_-][\mathbf{H}] & [\mathbf{A}_-][\mathbf{H} + \mathbf{G}_-] \end{bmatrix}\begin{bmatrix} \mathbf{F}_{w+} \\ \mathbf{F}_{w-} \end{bmatrix}$$

From the above, the characteristic equation is given by

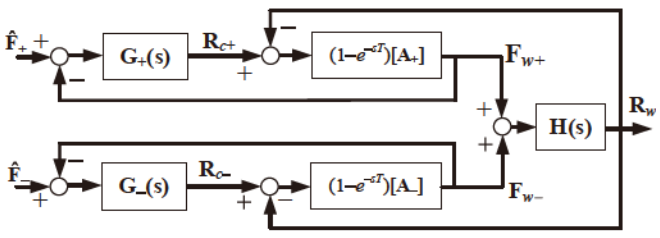

Fig. 4. Block diagram illustrating cutting dynamics.

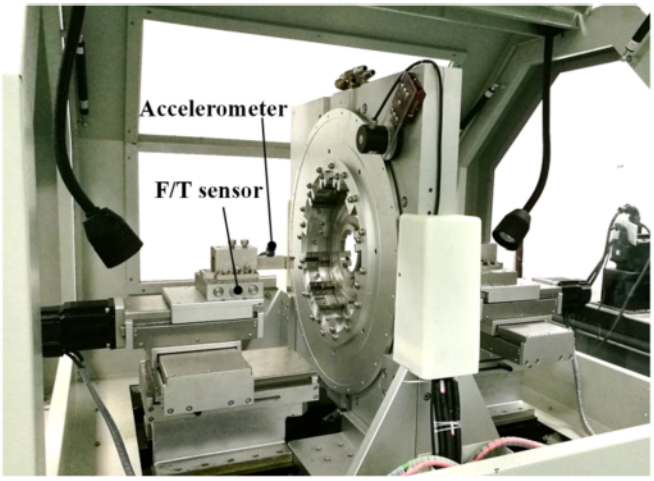

Fig. 5. DFT machine and experimental setup.

$$\det\left|[\mathbf{I}]_{6\times6} + (1-e^{-sT})\begin{bmatrix}\mathbf{A}_+(\mathbf{G}_+ + \mathbf{H}) & \mathbf{A}_+\mathbf{H} \\ \mathbf{A}_-\mathbf{H} & \mathbf{A}_-(\mathbf{G}_- + \mathbf{H})\end{bmatrix}\right| = 0 \tag{11}$$

It can be shown that the characteristic equation (11) can also be derived from Fig. 4 using a block-diagram reduction technique. With (10), $s = j\omega$ and $T = 60/n$, the characteristic equation (11) can be re-written explicitly in terms of n and $b_\pm$:

$$1 + (1 - e^{-j\omega\frac{60}{n}})\chi_1(b_+, b_-) + (1 - e^{-j\omega\frac{60}{n}})^2\chi_2(b_+, b_-) = 0 \tag{12}$$

where $\chi_1(b_+, b_-)=$

$$(b_+ + b_-)K_X(G_x + H_x) + (b_+\sigma_+ + b_-\sigma_-)K_Z(G_z + H_z)$$

and $\chi_2(b_+, b_-)=$

$$\begin{bmatrix} b_+b_-K_X^2(G_x^2 + 2G_xH_x) + \sigma_+b_+\sigma_-b_-K_Z^2(G_z^2 + 2G_zH_z) \\ +b_+b_-K_XK_Z(\sigma_+ + \sigma_-)(G_xG_z + G_xH_z + G_zH_x + 2H_xH_z)\end{bmatrix}$$

As characterized in (12), the dynamic cutting process of the DFT operation is a non-minimum phase system. Due to the zero-component in (5c), the transfer functions in the Y direction vanish in (12).

To help gain insights into the characteristic equation (12), the following notations are defined in (13) to facilitate discussions:

$$b_+ = b \text{ and } b_- = b + \hat{b} \tag{13}$$

$$\sigma_+b_+ = \sigma b = b_\sigma \text{ and } \sigma_-b_- = b_\sigma + \hat{b}_\sigma$$

where $\hat{b}_\sigma = (\hat{b} - R_n)\tan\psi$

The effects of the DFT on chatter can be broadly classified into the following three cases:

Case 1 Single-sided face-turning, $b_+ = b$ and $b_- = 0$.

Case 2 Symmetric DFT$b_\pm = b, \sigma_\pm b_\pm = \sigma b = b_\sigma, \hat{b} = \hat{b}_\sigma = 0$.

Case 3 Non-symmetric DFT ($\hat{b}$ and $\hat{b}_\sigma \neq 0$).

Case 1 (single-sided facing turning) provides a basis for comparison; and Cases 2 and 3 compare the dynamic effects of symmetric and non-symmetric DFT on chatter. With (13), the characteristic equation (12) for the three cases can be compactly expressed in terms of the DOC difference ($\hat{b}$ and $\hat{b}_\sigma$):

$$\chi_1(b, b_\sigma) = \begin{cases} \alpha(b, b_\sigma) & \text{Case 1} \\ 2\alpha(b, b_\sigma) & \text{Case 2} \\ 2\alpha(b, b_\sigma) + \alpha(\hat{b}, \hat{b}_\sigma) & \text{Case 3} \end{cases} \tag{14}$$

where $\alpha(b, b_\sigma) = bK_X(G_X + H_X) + b_\sigma K_Z(G_Z + H_Z)$

$$\chi_2(b, b_\sigma) = \begin{cases} 0 & \text{Case 1} \\ \beta(b, b_\sigma) & \text{Case 2} \\ \beta(b, b_\sigma) + \beta(b\hat{b}, b_\sigma\hat{b}_\sigma) & \text{Case 3} \end{cases} \tag{15}$$

where $\beta(b, b_\sigma) = \alpha^2(b, b_\sigma) - (bK_XH_X - b_\sigma K_ZH_Z)^2$

Using the Nyquist stability criterion [19], the stable cutting conditions for the DFT process can be determined from (12) along with (14) and (15). For a given system configuration (transfer functions, CT geometry, and WP material/geometry), the real and imaginary parts of the characteristic equation (12) as $\omega = 0 \to \infty$ can be plotted in the complex plane for a specified set of cutting parameters ($b_\pm$ and n). According to the Nyquist criterion, the cutting process is unstable with chatter if the Nyquist plot encircles the origin (or encircles -1 if 1 is dropped from the characteristic equation (12)). Therefore, a stability lobe can be constructed by scanning through the range of the spindle speeds and the DOCs in the cutting region of interest.

3. Results and discussions

The results of the numerical/experimental investigations, which were conducted on the transmission-free DD-DFT machine as illustrated in the CAD model (Fig. 1c), are organized into two parts:

Table 1
DFT parameters.

WP (D, h) = (300, 2) mm
Material: TC4 (Ti−6Al−4V)
Young modulus: 113.3 GPa
Rotor: Aluminum
Clamp: Steel/Copper

CT *Holder:* SDJCR-2525M-11
Insert: DCMT 11T302-SM (ψ, φ, ϕ)=(−3, 0, 0)°, R_n = 0.2 mm
Feed-rate = 0.25 mm/s η = 60°;
K_f = 2033 N/mm²; K_n = 3177/mm².

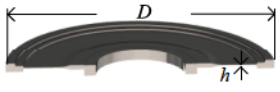

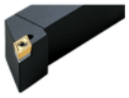

Cutting force coefficient verification

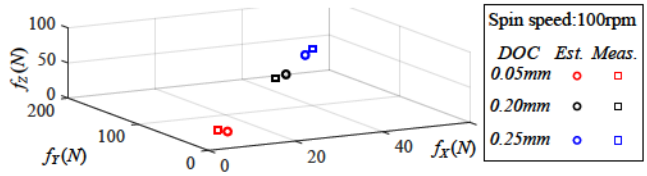

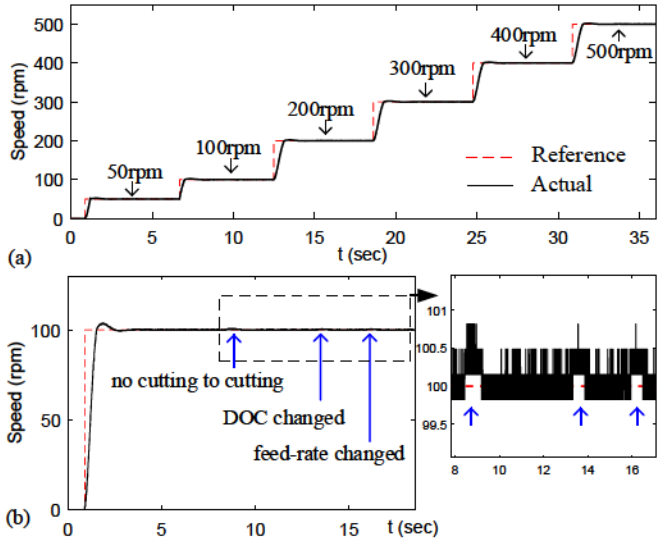

Fig. 6. Spindle speed test.

– The *first* part demonstrates the proposed DD spindle-motor for DFT of thin-walled disk-like WP, and identifies its system parameters and transfer functions for chatter prediction analyses.
– The *second* part illustrates the proposed chatter prediction method to obtain the stability lobe diagrams for the DFT process based on the Nyquist criterion.

The transmission-free DD-DFT machine that greatly reduces the system complexities as compared to its counterparts has been developed as shown in Fig. 5. Along with a cooling system embedded in the stator and the large number of distributed EMs (each sharing a small current and hence heat dissipation) on well-ventilated surfaces, heat problems commonly encountered in direct-drive motors are effectively overcome. While capable of offering high spin-torque at low speeds with precise speed-regulation typically required for manufacturing of hard-to-machine materials (such as titanium-alloy typically machined around a cutting line speed of 1 ~ 2 m/s), the structurally smart design potentially reduces mechanical vibrations and risks of system fault. The parameters (based on a titanium-alloy compressor disk) of the WP and CTs used in the validation of the DFT chatter prediction and in the numerical/experimental investigations of the DD-DFT machine are listed in Table 1. The cutting force coefficients (K_f, K_n) were extracted

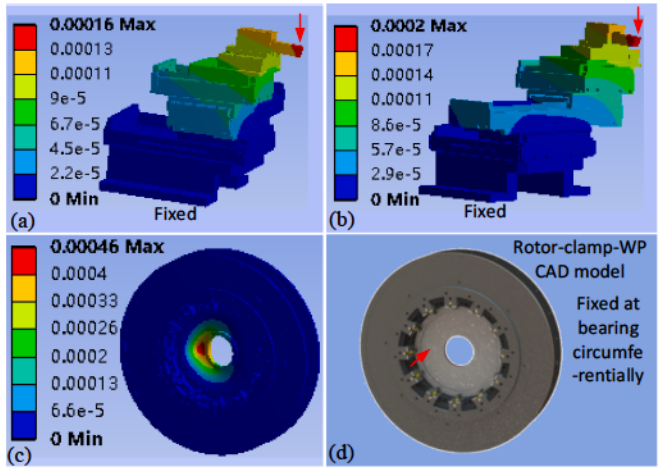

Fig. 7. Static deformation (mm), arrows denote force application points (a) CT stage: $X = Z = 0$ (b) CT stage: X, Z at maxima. (c) Rotor-WP assembly (d) CAD model for reference.

Table 2
WP Z-deformation for different cutting configurations.

Configuration	f_{z+}	f_{z-}	Δf_z ($f_{z+} - f_{z-}$)	Z-deformation
One-sided	100 N	0 N	100 N	46 μm
Symmetric DFT	100 N	100 N	0 N	0 μm
Non-symmetric DFT	100 N	90 N	10 N	4.6 μm

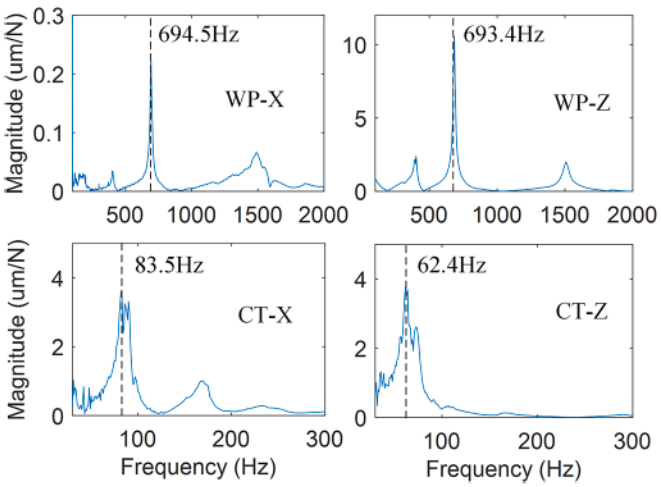

Fig. 8. FRFs of the WP-rotor and CT stage.

Table 3
FRF parameters.

$$G(s) \text{ or } H(s) = \frac{\omega_n^2}{k(s^2 + 2\zeta\omega_n s + \omega_n^2)} \quad (16)$$

Subsystem FRFs		$\omega_n/(2\pi)$ (Hz)	ζ	k ($\times 10^6$N/m)
WP-Rotor	$H_x(j\omega)$	694.5	0.0082	276
	$H_z(j\omega)$	693.4	0.0086	5.46
CT-Stage	$G_x(j\omega)$	83.5	0.0245	5.90
	$G_z(j\omega)$	62.4	0.0266	5.13

The FRFs are measured at the locations denoted by the arrows in Fig. 7.

using regression method [19] with (2) based on the cutting forces measured with the force/torque sensor (see Fig. 5). The extracted cutting force coefficients were verified by comparing the estimated and measured forces at different DOCs as illustrated in Table 1, which shows good agreement.

3.1. DD-DFT validation and parameter identification

Three tests were performed on the DD-DFT machine:

a) The speed regulation of the DD motor was experimentally evaluated; Fig. 6.
b) Static deformations of the rotor-clamp-WP assembly and the CT stage were numerically analyzed using commercial (ANSYS) FEA software; Fig. 7 and Table 2.
c) Using frequency response methods, the system transfer functions for chatter prediction analysis were identified experimentally; Fig. 8 and Table 3.

Fig. 6(a) graphs the responses of the spindle motor, where the speeds were regulated in step-changes from 50 rpm to 500 rpm, which correspond to the cutting line-speed ranging from 0.8 m/s to 8 m/s. The ability of the DD-motor to reject external disturbances at a regulated speed during the cutting process of a titanium-alloy WP was demonstrated in Fig. 6(b) at 100 rpm, where the arrows indicate the instants at

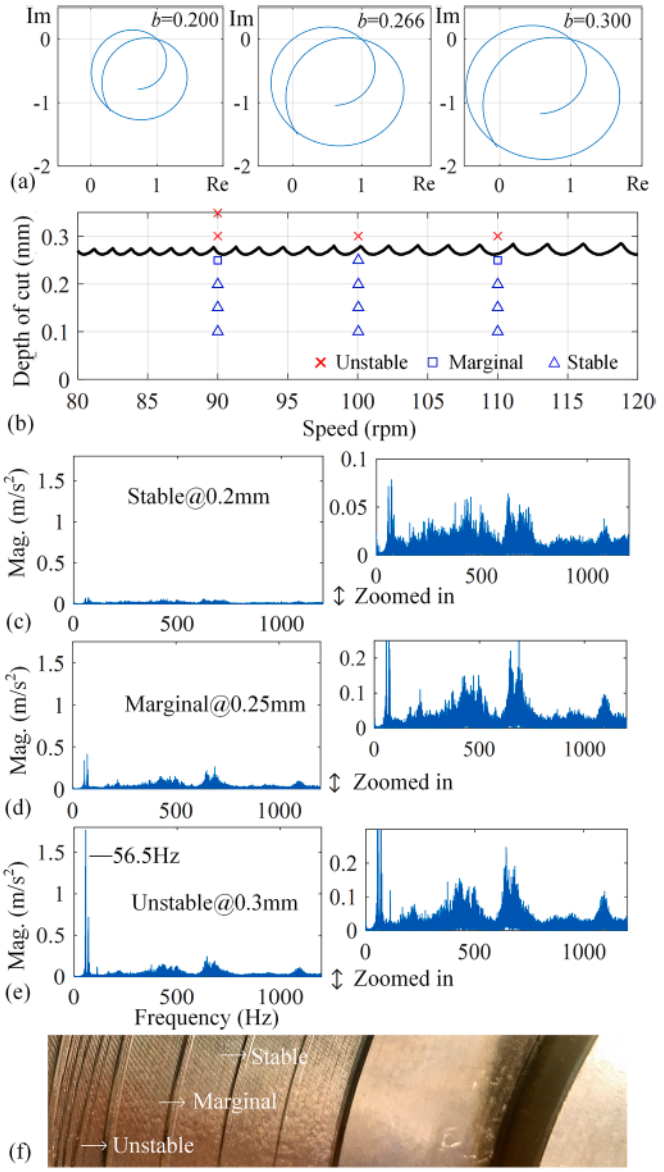

Fig. 9. Stability lobe and experimental verification of single-sided face turning (a) Nyquist plot, n = 90 rpm (b) Stability lobe (c) Acceleration spectra, stable (d) Acceleration spectra, marginal (e) Acceleration spectra, unstable (f) Illustration of machining surfaces.

which the cutting conditions changed.

The FEA stiffness analyses of the rotor-clamp-WP assembly and the CT stage are summarized in Fig. 7 where the arrows denote the locations at which the forces were applied. Fig. 7(a~c) show the deformations of the CT stage (at two CT positions) and the WP subjected to unit directional forces; the CAD model in Fig. 7(d) serves as a reference for visualization. Table 2 illustrates the relationship between the WP deformation and force conditions for the three cases discussed in Section 2.2, and compares the WP deformations along the Z-axis, which are characterized by distinct difference in normal forces.

Fig. 8 presents the frequency responses of the WP and CT in X- and Z-directions obtained using experimentally modal tests performed on the DFT machine (Fig. 5), based on which the frequency response functions (FRFs, when $s = j\omega$) were identified for the chatter prediction in (12). During the experiment, the WP-rotor and CT stages were excited using an impact hammer, where the impact locations were denoted by the arrows in Fig. 7. With the signals of the impact forces measured by the hammer integrated sensor and the vibrations recorded using an accelerometer (see Fig. 5), the FRFs were obtained using

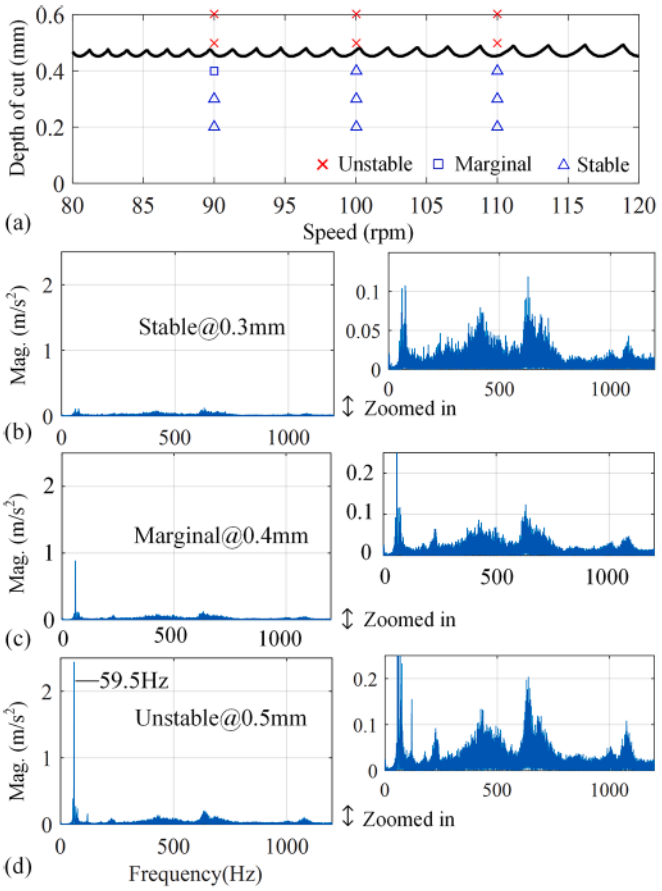

Fig. 10. Stability lobe and experimental verifications of symmetric DFT (a) Stability lobe, total DOC on both sides (b) Acceleration spectra, stable (c) Acceleration spectra, marginal, (d) Acceleration spectra, unstable.

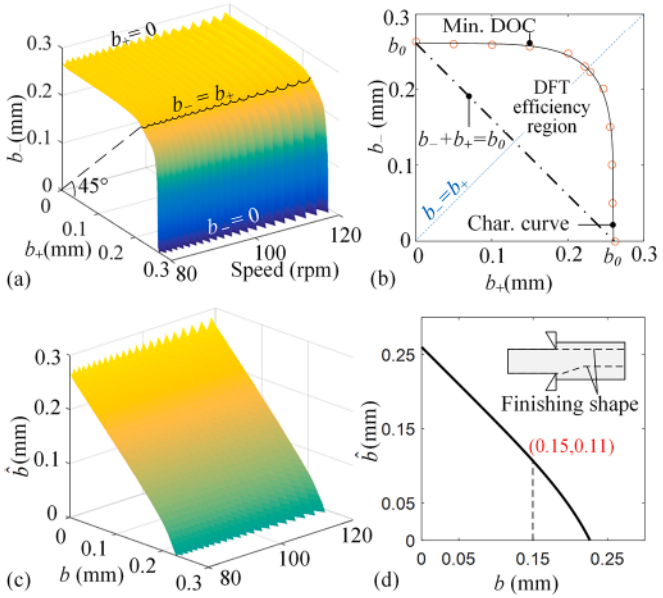

Fig. 11. Illustration non-symmetric DFT (a) Stability surface and (b) characteristic curve in terms of independently specified DOC. (c) Stability surface and (d) characteristic curve based on the nominal DOC and its difference between the two sides of the WP.

Fourier analyzer and modal analysis method [19]. Based on the frequency responses in Fig. 8, the parameters of the FRFs that have the form of (16) were identified which are listed in Table 3.

The above results are analyzed and discussed:

- The DD-motor can provide precise speed regulation in a wide range with robust performance at disturbances, verifying the capability of the spindle motor for machining hard-to-machine materials (such as titanium-alloy) that require large spin torques at low speeds.
- The CT stage at different CT positions exhibit similar stiffness (Fig. 7a and b). The deformations of the clamp and the rotor are negligible as compared with that of the WP. As illustrated in Fig. 7(c) and the CAD model in Fig. 7(d), the small-thickness web of the WP has relatively low stiffness, which tends to deform along the *Z*-direction when subjected to unbalanced normal forces. As the normal forces exerted by the CTs from the opposite sides of the WP fully (or partially) cancel out each other in the DFT process, the WP deformation in DFT process is much smaller than that in one-sided cutting process, as suggested by the results in Table 2.

3.2. Stability lobe analysis and verifications

With the experimentally identified FRFs and parameters in Table 3, the stability lobe diagrams for the DFT process were obtained using Nyquist criterion based on the characteristic equations (12), (14) and (15) derived in Section 2.2. With the above findings, the proposed DFT chatter prediction method was experimentally verified with cutting tests. The results are organized as follows:

1. Single-sided turning: $b_+ = b$, $b_- = 0$; Fig. 9.
2. Symmetric DFT: $b_+ = b_- = b$; Fig. 10.
3. Nonsymmetrical DFT: Independent b_+ and b_-; Fig. 11.

Fig. 9 demonstrates the procedure of the proposed DFT chatter prediction where results were computed for Case 1 (single-sided turning) for different spindle speeds and DOCs. To facilitate illustration and for visualization, Fig. 9(a) depicts the real and imaginary parts of the characteristic equation (12) in the complex plane for $b = 0.200$, 0.266 and 0.300 mm at $n = 90$ rpm. According to Nyquist criterion, the cutting process is unstable with chatter if the polar plot encircles the origin ($b = 0.300$). The critical stability occurs when the polar plot passes the origin ($b = 0.266$). For $b < 0.266$, the process is stable ($b = 0.2$). The stability inspection was repeated by scanning the range of spindle speeds and that of DOCs; the computed stability lobe is shown in Fig. 9(b). Specifically, the stability lobe shows the critical DOC for the spindle speed ranging from 80 to 120 rpm, corresponding to a cutting line speed ranging from 1.3 to 1.9 m/s. To verify the stability lobe, cutting tests were performed and the results are super-imposed in Fig. 9(b) for comparison which shows good agreements. The spectra of the vibrations during the cutting tests (recorded using accelerometer) and the surface qualities are shown in Fig. 9(c ~ e) for stable, marginal and unstable cuttings respectively. It can be seen that the chatter had a frequency at 56.5 Hz when unstable cutting occurred, which is close to the natural frequency of the CT in *Z*-axis (62.4 Hz).

Similarly, the stability lobe were obtained for the Case 2 (symmetric DFT). The results, which were verified with cutting tests by simultaneously setting the DOCs for both CTs, are shown in Fig. 10(a), suggesting that the stability lobe agrees very well with the results of the cutting tests. The vibration spectra were plotted in Fig. 10(b ~ d).

Fig. 11 illustrates the effects of nonsymmetrical DFT for machining WPs with nonsymmetrical surfaces on the stability diagram. In Fig. 11(a) where the results are computed using (12) with two independently specified DOCs (b_+ and b_-), the surface characterizes the pair of critical DOCs (b_+ and b_-) at a specified spindle speed. As shown in Fig. 11(a), the region enclosed by the surface (in the first quadrant) is stable. The improved efficiency of the DFT process over the single-side cutting can be illustrated by Fig. 11(b) where the open circles are the minimum (b_+, b_-) values in the specified speed range extracted from the critical surface for a DFT process in Fig. 11(a). The extracted points characterizing the relationship between b_+ and b can be curve-fit by (17) where b_0 is the equivalent DOC of the single-sided cutting:

$$b_+^a + b_-^a = b_0^a, \quad 0 \le b_+, b_- \le b_0 \tag{17}$$

where $a = 5$ and $b_0 = 0.262$. Alternatively, the stability surface for Case 3 can be obtained using (12) along with (14) and (15). Similar stability surface and characteristic curve are plotted in Fig. 11(c and d) but as a function of b and $\hat{b}$ to provide a quick guide for nonsymmetrical DFT in the specified speed range.

The analysis based on the results from Figs. 9–11 are summarized:

- Fig. 11(b) offers a quick guide to determine the machining parameters for DFT in the specified speed range, where the stable cutting region can be divided into two parts by the straight line ($b_0 = b_+ + b_-$) that represents the total MRR on both sides equal to the equivalent MRR of Case 1 (where the face-turning takes place only on one side). The area above this straight line but bounded by the characteristic curve (17) represents the region of improved efficiency where the DFT is more efficient than traditional single-sided turning. For symmetrical DFT (Case 2 where $b_+ = b_-$), the maximum MRR can be approximately characterized by $(b_+ + b_-) = 1.75 b_0$.
- The characteristic curve in Fig. 11(d) provides a quick guide for nonsymmetrical DFT in the specified speed range. Fig. 11(d) illustrates an example when a transition from symmetric DFT to non-symmetric DFT is required. In this example, the DOCs for both sides of the WP are 0.15 mm initially, and one side must change (per the finishing face shape variation); guided by Fig. 11(d), the DOC change margin is 0.11 mm.

4. Conclusions

This paper presents a DFT machine featured with a direct-drive spindle motor and duplex symmetric cutters for manufacturing disk-like WPs with reduced deformations and improved surface quality. The transmission-free spindle is capable of precise speed regulation in a wide range and low vibration operation. A chatter stability analysis method has been proposed by formulating the multi-dimensional dynamic cutting force models of the DFT process, where the dynamics of both WP and the cutters are taken into account. The stability limit computed using the proposed method with parameters experimentally identified from the DFT machine has been experimentally verified and the DFT process has been evaluated based on the machining of hard-to-machine (titanium-alloy) disks with a diameter-to-thickness ratio of 150. The test results conducted on singled-sided, symmetric-DFT and nonsymmetric-DFT demonstrate that the DFT can effectively increase the system stability limit; and the critical DOC has been increased by as large as 1.75 times with symmetric DFT compared to one-sided face turning. The proposed method also provides a computationally efficient way for planning the turning procedures of disk-like WPs with symmetric or non-symmetric faces where the DOCs on each side can be determined with a pre-computed curve-fit function.

Acknowledgement

This work was supported in part by the National Basic Research Program of China (973 Program) under Grant 2013CB035803, U. S. National Science Foundation under Grant CMMI-1662700 and National Science Foundation of China under Grant 51675194.

References

[1] J. Guo, K.-M. Lee, W. Liu, B. Wang, Design criteria based on modal analysis for vibration sensing of thin-wall plate machining, IEEE ASME Trans. Mechatron. 20/3 (2015) 1406–1417.
[2] Y. Altintas, E. Budak, Analytical prediction of stability lobes in milling, CIRP Annals 44/1 (1995) 357–362.
[3] M. Eynian, Y. Altintas, Chatter stability of general turning operations with process damping, J. Manuf. Sci. Eng. 131/4 (2009) 041005-041005.

[4] Y. Kurata, S.D. Merdol, Y. Altintas, N. Suzuki, E. Shamoto, Chatter stability in turning and milling with in process identified process damping, J. Adv. Mech. Des., Sys. Manuf. 4 (2010) 1107–1118.
[5] M. Siddhpura, R. Paurobally, A review of chatter vibration research in turning, Int. J. Mach. Tool Manufact. 61 (2012) 27–47.
[6] J. Munoa, X. Beudaert, Z. Dombovari, Y. Altintas, E. Budak, C. Brecher, G. Stepan, Chatter suppression techniques in metal cutting, CIRP Annals 65/2 (2016) 785–808.
[7] B.C. Rao, Y.C. Shin, A comprehensive dynamic cutting force model for chatter prediction in turning, Int. J. Mach. Tool Manufact. 39/10 (1999) 1631–1654.
[8] E. Budak, E. Ozlu, Analytical modeling of chatter stability in turning and boring operations: a multi-dimensional approach, CIRP Ann. - Manuf. Technol. 56 (2007) 401–404.
[9] B.E. Clancy, Y.C. Shin, A comprehensive chatter prediction model for face turning operation including tool wear effect, Int. J. Mach. Tool Manufact. 42/9 (2002) 1035–1044.
[10] M.J. Reith, G. Stepan, Effect of non-proportional damping on the dynamics and stability of multi-cutter turning systems, Int. J. Mach. Tool Manufact. 117 (2017) 23–30.
[11] C. Brecher, A. Epple, S. Neus, M. Fey, Optimal process parameters for parallel turning operations on shared cutting surfaces, Int. J. Mach. Tool Manufact. 95 (2015) 13–19.
[12] E. Budak, A. Comak, E. Ozturk, Stability and high performance machining conditions in simultaneous milling, CIRP Ann. 62/1 (2013) 403–406.
[13] E. Shamoto, T. Mori, K. Nishimura, T. Hiramatsu, Y. Kurata, Suppression of regenerative chatter vibration in simultaneous double-sided milling of flexible plates by speed difference, CIRP Ann. 59/1 (2010) 387–390.
[14] E. Budak, E. Ozturk, Dynamics and stability of parallel turning operations, CIRP Ann. - Manuf. Technol. 60 (2011) 383–386.
[15] M. Azvar, E. Budak, Multi-dimensional chatter stability for enhanced productivity in different parallel turning strategies, Int. J. Mach. Tool Manufact. 123 (2017) 116–128.
[16] E. Ozturk, A. Comak, E. Budak, Tuning of tool dynamics for increased stability of parallel (simultaneous) turning processes, J. Sound Vib. 360 (2016) 17–30.
[17] K. Bai, K.-M. Lee, J. Cao, B. Hao, Analytical development of a minimum bearing reaction twin-motor for duplex machining, 2015 IEEE International Conference on Advanced Intelligent Mechatronics, 2015, pp. 1457–1462.
[18] K. Bai, K.-M. Lee, J. Cao, R. Xu, L. Li, Design and decoupled compensation methods of a PM motor capable of 6-D force/torque actuation for minimum bearing reaction, IEEE ASME Trans. Mechatron. 22/5 (2017) 2252–2264.
[19] Y. Altintas, Manufacturing Automation, second ed., Cambridge University Press, 2012.